Magnetic phase diagram of underdoped $YBa_2Cu_3O_y$ inferred from torque magnetization and thermal conductivity

Fan Yu[a], Max Hirschberger[b], Toshinao Loew[c], Gang Li[a], Benjamin J. Lawson[a], Tomoya Asaba[a], J. B. Kemper[d,e,2], Tian Liang[b], Juan Porras[c], Gregory S. Boebinger[d,e], John Singleton[f], Bernhard Keimer[c], Lu Li[a], and N. Phuan Ong[b,1]

[a]Department of Physics, University of Michigan, Ann Arbor, MI 48109; [b]Department of Physics, Princeton University, Princeton, NJ 08544; [c]Max Planck Institute for Solid State Research, 70569 Stuttgart, Germany; [d]Department of Physics, Florida State University, Tallahassee, FL 32310; [e]National High Magnetic Field Laboratory, Florida State University, Tallahassee, FL 32306; and [f]National High Magnetic Field Laboratory, Los Alamos National Laboratory, Los Alamos, NM 87545

Contributed by N. Phuan Ong, September 16, 2016 (sent for review August 2, 2016; reviewed by Patrick A. Lee and John M. Tranquada)

Strong evidence for charge-density correlation in the underdoped phase of the cuprate $YBa_2Cu_3O_y$ was obtained by NMR and resonant X-ray scattering. The fluctuations were found to be enhanced in strong magnetic fields. Recently, 3D charge-density–wave (CDW) formation with long-range order (LRO) was observed by X-ray diffraction in $H > 15$ T. To elucidate how the CDW transition impacts the pair condensate, we have used torque magnetization to 45 T and thermal conductivity κ_{xx} to construct the magnetic phase diagram in untwinned crystals with hole density $p = 0.11$. We show that the 3D CDW transitions appear as sharp features in the susceptibility and κ_{xx} at the fields H_K and H_p, which define phase boundaries in agreement with spectroscopic techniques. From measurements of the melting field $H_m(T)$ of the vortex solid, we obtain evidence for two vortex solid states below 8 K. At 0.5 K, the pair condensate appears to adjust to the 3D CDW by a sharp transition at 24 T between two vortex solids with very different shear moduli. At even higher H (41 T), the second vortex solid melts to a vortex liquid which survives to fields well above 41 T. de Haas–van Alphen oscillations appear at fields 24–28 T, below the lower bound for the upper critical field H_{c2}.

cuprate superconductivity | high-field phase diagram | vortex liquid | torque magnetometry | thermal conductivity

The existence of static charge order in underdoped $YBa_2Cu_3O_y$ (YBCO) in an intense magnetic field was reported by Wu et al. (1) using NMR. Subsequently, Ghiringhelli et al. (2) uncovered temperature-dependent charge-density–wave (CDW) correlations in zero magnetic field by resonant X-ray scattering (RXS). The RXS signal onsets near 180 K and peaks at the superconducting critical temperature T_c before falling. Several groups (3–5) recently showed that the RXS intensity is enhanced in finite field H. At low temperature T, several experiments have uncovered field-induced transitions. These include a transition at 18 T from ultrasonic measurements (6), features in the high-field thermal conductivity (7), and the onset of line splitting in the NMR spectra starting at the charge-ordering field $H_{ch} = 10$–15 T and saturating at around 18–20 T (depending on the hole density p) (8). Recent X-ray diffraction experiments (9–11) show that the transition to a 3D CDW with long-range order (LRO) onsets near $H = 15$ T.

The field-induced CDW state raises several intriguing questions regarding its relation to superconductivity. Does CDW formation with LRO suppress the superconducting condensate? Where is the true upper critical field H_{c2}? How does it affect the stability of the vortex solid? Although NMR and X-ray diffraction are incisive probes of charge modulation and CDW formation, they do not couple directly to the fundamental excitations of the pair condensate (quasi-particles and vortices), so they are less sensitive to the pairing correlations which reflect superconductivity. By contrast, the diamagnetic magnetization $\mathbf{M}_d$ (which dominates the observed magnetization $\mathbf{M}_{obs}$ below the critical temperature T_c) couples directly to the vortex excitations because it measures the current–current correlation. In the magnetic phase diagram, hysteretic behavior of the $\mathbf{M}_d$ curves readily identifies the stability region of the vortex solid. Above the melting field of the solid H_m, $\mathbf{M}_d$ also identifies the vortex liquid which displays a unique reversible diamagnetism. Surprisingly, we find that the magnetic susceptibility χ_d also detects the onset of charge ordering as a weak peak at the field H_K. Both H_K and a higher cross-over field H_p are apparent in the thermal conductivity. We compare H_K and H_p with field scales reported from NMR and ultrasonic experiments. Taken together, these features fill out the magnetic phase diagram, and relate the charge-ordering fields to the phase boundaries in the vortex system.

We have measured by high-resolution torque magnetometry the magnetization and thermal conductivity κ_{xx} in high-purity, detwinned ortho-II crystals of $YBa_2Cu_3O_y$ ($y = 6.55$, $T_c = 61$ K, $p = 0.11$) in a dc field H up to 45 T. Sample 1 has a large volume to facilitate accurate measurements at T up to 210 K. Sample 2 and sample 3 were picked to have smaller volumes (0.184 mm^3 and 0.344 mm^3, respectively) to avoid overloading the cantilever in the vortex solid regime below T_c (see ref. 4 for details on the crystals). Samples 4 and 5 were used for the κ_{xx} measurements. From

Significance

We obtain the magnetic phase diagram in the underdoped cuprate $YBa_2Cu_3O_y$ using torque magnetometry at temperatures 0.3–70 K and magnetic fields up to 45 T. At low fields, vortices (quantized flux tubes) form a vortex solid that is strongly pinned to the lattice. At large fields, melting of the solid to a vortex liquid produces nonzero dissipation. However, the vortex liquid persists to fields above 41 T. We have also mapped out the "transition" fields at which the charge-density–wave state (observed in X-ray diffraction experiments) becomes stable. Our results show that, in intense fields, superconductivity adjusts to coexist with the charge-density wave, but the Cooper pairs, which define the superconducting fluid, survive to fields well above 41 T.

Author contributions: F.Y., G.S.B., L.L., and N.P.O. designed research; F.Y., M.H., G.L., B.J.L., T.A., J.B.K., T. Liang, J.S., L.L., and N.P.O. performed research; T. Loew, J.P., and B.K. contributed new reagents/analytic tools; F.Y., M.H., G.L., B.J.L., T.A., T. Liang, L.L., and N.P.O. analyzed data; T. Loew and J.P. grew and characterized the crystals used; J.B.K. assisted in developing high-field experimental techniques; G.S.B. helped to understand experimental results; J.S. developed pulsed-field magnetization techniques; B.K. supplied high-quality crystals; and M.H., B.K., L.L., and N.P.O. wrote the paper.

Reviewers: P.A.L., Massachusetts Institute of Technology; and J.M.T., Brookhaven National Laboratory.

The authors declare no conflict of interest.

[1]To whom correspondence should be addressed. Email: npo@princeton.edu.

[2]Present address: Department of Physics, Gonzaga University, Spokane, WA 99258.

This article contains supporting information online at www.pnas.org/lookup/suppl/doi:10.1073/pnas.1612591113/-/DCSupplemental.

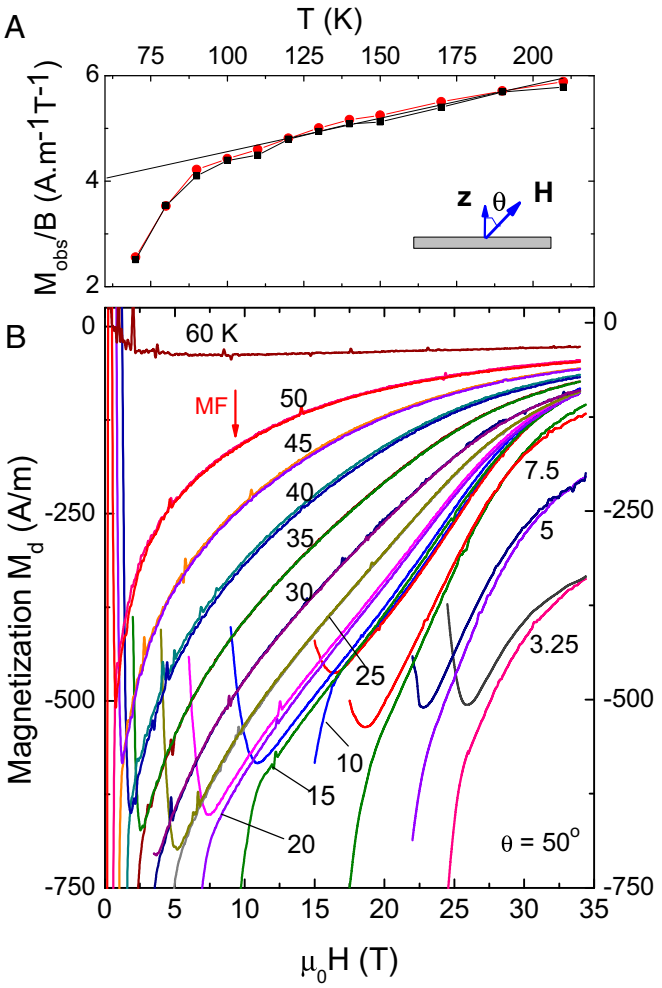

Fig. 1. Magnetization in ortho-II $YBa_2Cu_3O_y$ ($y = 6.55$, $T_c = 61$ K, $P = 0.11$) measured by torque magnetometry in dc field. (*A*) Observed susceptibility M_{obs}/B from $T = 80$–210 K measured at 8 T (black circles) and 11 T (red) in sample 1 ($B = \mu_0 H$, with μ_0 the permeability). The straight line is the Van Vleck anisotropy background $\Delta\chi^v = a(T + T_0)$ with $a = 1.18 \times 10^{-2}$ A(mTK)$^{-1}$ and $T_0 = 305$ K. The diamagnetic term M_d onsets near 110 K. (*Inset*) Tilt angle θ between **H** and the normal $\hat{z} \| \hat{c}$. (*B*) $M_d(T, H) = M_{obs}(T, H) - a(T + T_0)H$ vs. the magnetic field $\mu_0 H$ measured at selected T in sample 2 with $\theta = 50°$. Splitting of the sweep-up from the sweep-down curves occurs at the melting field $H_m(T)$. At each T, the sample is in the vortex liquid state for $H > H_m(T)$. Diamagnetism persists to fields significantly above 32 T. For the curve at 50 K, the red arrow (labeled "MF") marks the $H_{c2,MF}/\cos\theta$ using the mean-field value suggested for H_{c2} (7).

120 to 210 K (Fig. 1*A*), the torque magnetization M_{obs} arises predominantly from the anisotropy $\Delta\chi^v = \chi_c^v - \chi_a^v$ of the paramagnetic Van Vleck term (χ_i^v is the susceptibility along axis i) (12, 13). $\Delta\chi^v(T)$ has a weak T dependence $\Delta\chi^v = a(T + T_0)$, with $T_0 = 305$ K (*SI Appendix*, section S1). At 110 K, we start to resolve a negative contribution caused by fluctuating diamagnetism. As $T \to T_c$, the diamagnetic component M_d grows rapidly in magnitude. In Sample 2, we focused on measurements of M_{obs} to 34 T at selected T between 10 and 80 K. In nonsuperconducting $La_{2-x}Sr_xCuO_4$ ($x = 0.050$), the Van Vleck term retains the form $a(T + T_0)$ down to 10 K (12). Hence, to isolate M_d we subtract this term from M_{obs}, i.e., $M_d(T, H) = M_{obs}(T, H) - a(T + T_0)H$.

Diamagnetism in the Vortex Liquid State

Fig. 1*B* displays the curves of M_d vs. H measured at temperatures from 60 K down to 3.25 K in fields up to 34 T with tilt angle $\theta = 50°$. At all $T < 60$ K, M_d is negative (diamagnetic) but increases rapidly with H. Throughout most of the field scale shown, the curves are reversible (sweep-up and sweep-down traces coincide). The reversible, strongly T-dependent diamagnetic response is the hallmark of the vortex liquid. Throughout the vortex liquid regime, $|M_d|$ is far too large to be attributed to Gaussian fluctuations (100 A/m corresponds to 1.8×10^{-3} Bohr magneton per unit cell). The diamagnetic signal reflects the array of small, diamagnetic supercurrent loops occupying the interstitial space between vortex cores. At each T, bifurcation of the sweep-up and -down curves occurs at the melting field $H_m(T)$ which separates the vortex solid from the liquid (at the scale shown, this first becomes apparent at 45 K at $\sim$ 1.5 T). As T decreases, $H_m(T)$ rises rapidly, reaching 25 T at 3.25 K. (As sketched in Fig. 1*A*, **H** is aligned at an angle θ to the c axis of the crystal. We define $\mathbf{H} \cdot \hat{\mathbf{c}} = H_z$.)

Peak in the Differential Susceptibility

An important feature of the M_d –H curves is the inflection (or kink) near $H = 25$ T for T below 20 K. The inflection is observed as a weak maximum in the differential susceptibility $\chi_d = dM_d/dB$, with B the flux density. Fig. 2 shows the curves of χ_d vs. H in measurements taken up to 45 T (sample 3) at selected values of the field tilt angle θ from 9° to 65° with T fixed at 15 K. The peaks are observed in the reversible part of the vortex phase diagram (solid and dashed curves were recorded in the field sweep-up and -down directions, respectively). We refer to the maxima in χ_d at each θ as the field $H_{K,\theta}$ (identified by vertical arrows in Figs. 2, 3*B*, and 4). (In the curves of χ_d vs. H plotted in Fig. 3*B*, the broad peak sits on a gentle linear background. The background does not affect

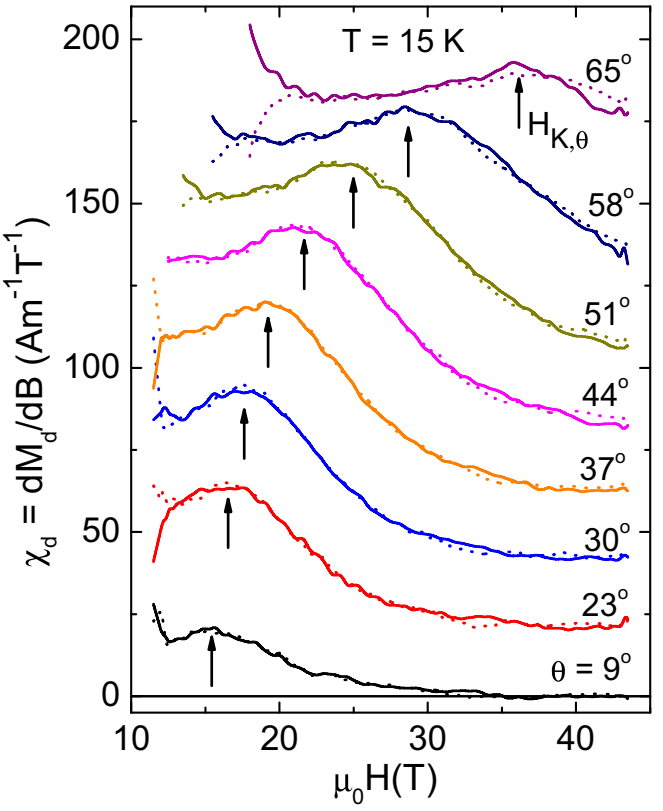

Fig. 2. Differential magnetic susceptibility $\chi_d \equiv dM_d/dB$ of YBCO (sample 3) is plotted against the magnetic field H at selected tilt angles θ at $T = 15$ K. The curves have been shifted vertically for clarity. At each θ, the solid (dashed) curve was recorded while the field H was slowly swept up (down). The bifurcation of the curves at low fields defines the melting field H_m of the vortex solid to the liquid state. In the liquid state, the χ_d –H curves display a broad peak which defines the field $H_{K,\theta}$ (arrows).

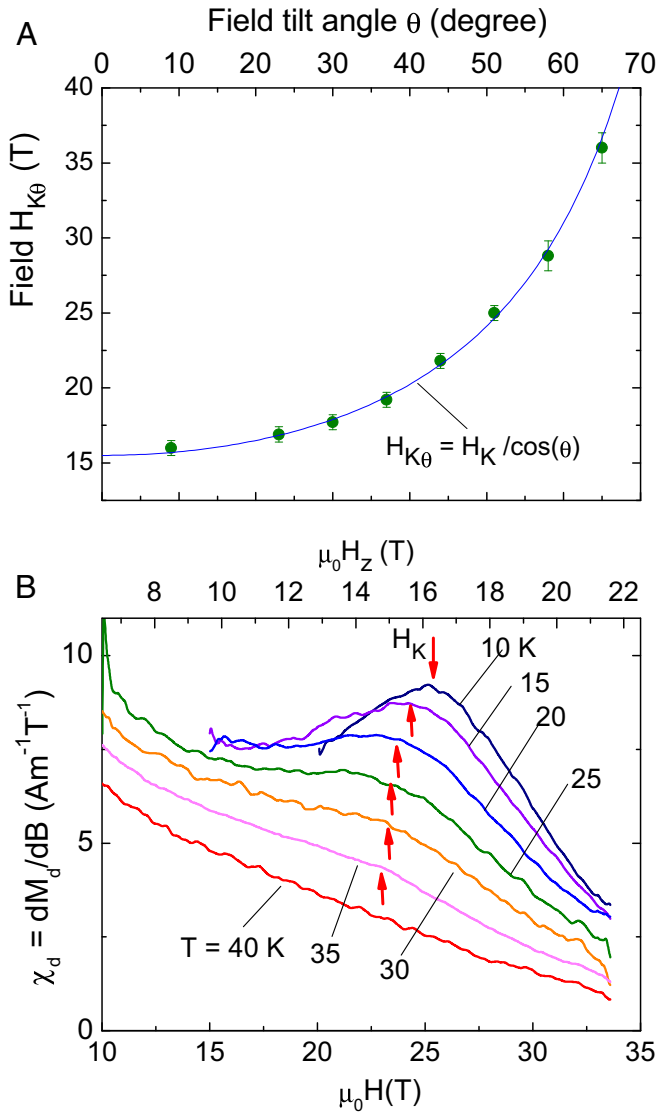

Fig. 3. (*A*) Angular dependence of the kink field $H_{K,\theta}$ at 15 K in sample 3 identified by the arrows in Fig. 2. The solid line is a fit to the sinusoidal expression $H_{K,\theta} = H_K/\cos\theta$, with $H_K \simeq 16$ T. (*B*) Field profiles of the differential susceptibility χ_d at selected T from 10 to 40 K measured in sample 2 with θ fixed at 50°. The lower x axis displays the applied field H while the upper x axis displays the z-component H_z. At 40 K, χ_d is a featureless, decreasing function of H. Below 40 K, however, a broad peak becomes resolvable, with an amplitude that grows as $T \to 10$ K. The peak in χ_d varies only weakly with T from H_z = 15–16 T (red arrows).

the actual value of H_K, which can be determined from the change in sign of $d\chi_d/dB$.)

The strong angular dependence of $H_{K,\theta}$ in Fig. 2 suggests that it is mostly determined by the z component H_z of the field. In Fig. 3*A*, we plot the variation of $H_{K,\theta}$ vs. θ at 15 K. As θ increases, $H_{K,\theta}$ increases monotonically from ~15 T (at 10°) to values exceeding our maximum applied field of 45 T when θ exceeds 65°. By fitting the data to the sinusoidal form $H_{K,\theta} = H_K/\cos\theta$ (solid curve), we confirm that for each θ, the kink feature occurs when H_z equals a θ-independent field, which we call H_K. The peak signals an electronic transition that is driven predominantly by H_z. Below, we identify H_K with the onset of static charge ordering.

The field H_K inferred from χ_d hardly varies at all with T below 40 K. Fig. 3*B* plots the curves of χ_d vs. H measured in sample 2 at selected T from 40 to 10 K. At 40 K, the curve of χ_d is initially featureless. As we cool to 10 K, a broad peak appears at 10 K. As shown in the scale on the upper x axis, the peak (arrows) varies from 15 to 16 T. Fig. 4 plots curves of χ_d for T down to 3.25 K in sample 2. As we cool below 10 K, the rapid increase in melting field $H_m(T)$ causes the two fields to cross near 6 K, so that the H_K feature now occurs within the vortex solid state where the variation of M_d vs. H is steep and hysteretic. This precludes determination of H_K using the peak in χ_d. However, as we show next, we can track it inside the vortex solid region using the thermal conductivity.

Thermal Conductivity

We have measured thermal conductivity in samples 4 and 5 using a standard configuration with two thermometers and one resistive heater. The shorter edge of the rectangular sample platelet was rigidly attached to the heat bath with silver paint, standing upright in vacuum in an applied field $\mathbf{H}\|\mathbf{c}$. In sample 4, the heat current density $\mathbf{J}_Q$ was applied parallel to the axis **b** (the chain axis), whereas in sample 5 $\mathbf{J}_Q\|\mathbf{a}$ (Fig. 5). To distinguish the two axes, we define the longitudinal thermal conductivities as κ_b and κ_a, respectively ($\kappa_b > \kappa_a$), and suppress writing the tensor indices xx and yy. Note that below T_c, for $H = 0$, κ_b exceeds κ_a by a factor 1.3–1.4. In finite H, the factor is even larger at 4.5 K, as we show next.

The heater was glued directly on the crystal using silver paint, while the chip thermometers (Lakeshore Cryotronics Cernox

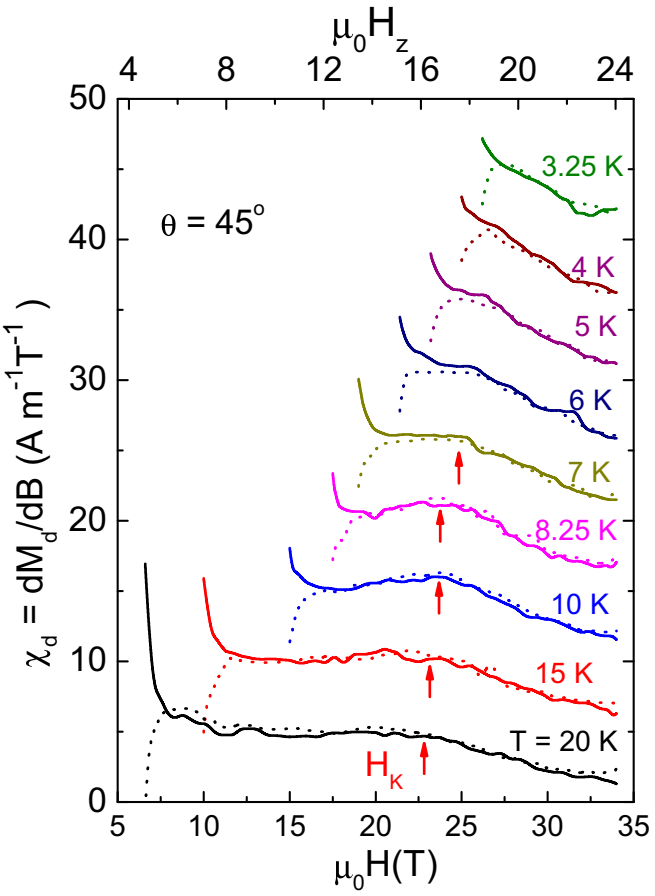

Fig. 4. Differential susceptibility $\chi_d = \partial M/\partial B$ plotted vs. the applied field H (lower x axis) and $H_z = H\cos\theta$ (upper) measured in sample 2 with $\theta = 45°$ at selected temperatures 3.25 K $\leq T \leq$ 20K. The curves have been shifted vertically for clarity. At each T, the solid curves (dashed curves) were recorded as H was slowly swept up (swept down). Below 6 K, the kink feature cannot be resolved against the large variations of hysteretic loops in the χ_d –H curves.

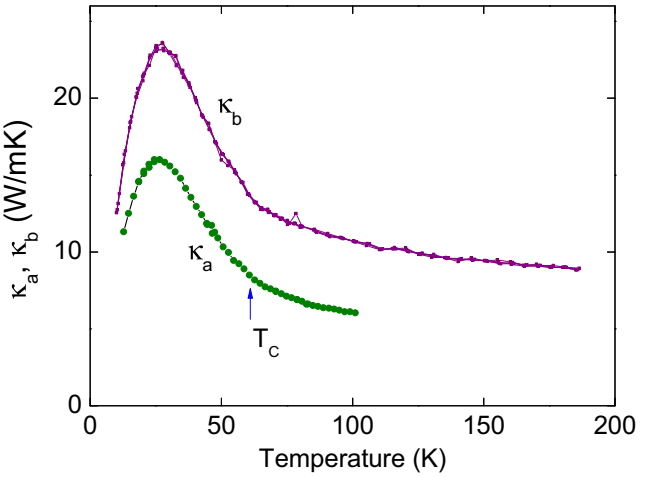

Fig. 5. The thermal conductivities κ_a (measured in sample 5) and κ_b (sample 4) in zero H.

CX1030 bare chip) were heat sunk to the crystal (using epoxy) via thick gold wires. Four thin phosphor-bronze wires were attached to each thermometer for a four-point resistance measurement. This configuration ensures good thermal contact and fast equilibration between the thermometers and the sample. The thermometers were carefully calibrated in situ, both in zero H and large H. The low-temperature setup including two reference thermometers on the sample stage was contained in a custom-made vacuum can inside the variable-temperature insert in a 35-T resistive magnet (*SI Appendix*, section S4).

The curves of κ_a and κ_b vs. H, plotted in expanded scale in Fig. 6, reveal two distinctive features (breaks in slope) that are nearly T-independent below 40 K (arrows). The feature at lower H may be identified with H_K because it occurs at the same field value to our resolution. The upper feature is called H_p. As T is raised, the features at H_K and H_p are thermally broadened, becoming unresolvable above 35 K. The step changes in κ_a and κ_b in the field interval (H_K, H_P) are quite small, accounting for <5% of the electronic thermal conductivity (*SI Appendix*, Fig. S6).

Magnetization to 45 T and de Haas–van Alphen Oscillations

The foregoing experiments, carried out to maximum fields of 35 T, pointed to intriguing features in the magnetic phase diagram which become better resolved at lower T and higher magnetic fields. We have extended the torque experiments to 45 T at temperatures down to 0.3 K and uncovered a distinct phase of the vortex system (vortex solid 2) that survives to 41 T. In addition, we have resolved de Haas–van Alphen (dHvA) oscillations (14) which onset in the vortex solid 2 phase [with amplitude and Dingle temperature closely similar to those in a previous dHvA experiment (15–17)]. We show that the vortex liquid appearing above the melting field is robust to H_z = 41 T (and well beyond judging from the trend vs. H).

Fig. 7 shows traces of the torque τ vs. H in the field region where the hysteretic loops begin to close at T = 0.5, 1.8, and 5 K. A number of important conclusions may be drawn from Fig. 7. First, the rapid closing of the hysteresis loop suggests that we can define a "lower" melting field H_{m1} (the nexus of the linear extrapolations of the upper and lower branches of τ). Above H_{m1}, there exists a second vortex solid phase ("vortex solid 2," in the shaded region) that has a much weaker shear modulus but survives to a higher melting field H_{m2}. As we cool from 5 to 0.5 K, the small shaded region expands rapidly (H_{m1} = 28 T and H_{m2} ~ 42 T at 0.5 K). The rapid growth suggests that the vortex solid 2 constitutes a distinctive, stable phase of the overall vortex solid in the limit $T \to 0$ (instead of a fluctuation tail).

Secondly, when the curves are nonhysteretic ($H > H_{m2}$), the magnetic response is strongly diamagnetic at all fields up to 45 T ($\tau < 0$). From the trends of the curves, the diamagnetic response extends to fields considerably above 45 T. Because reversible diamagnetism is a hallmark of the vortex liquid, we conclude that the vortex liquid and the underlying pair amplitude are stable to extremely high magnetic fields, well beyond either melting field. These observations confirm the conclusion from previous Nernst and torque experiments that the pairing strength in cuprates is extremely robust.

Finally, dHvA oscillations can be resolved even in the curves at 5 K (*SI Appendix*, section S3, Fig. S4). The onset of the oscillations at 0.5 K occurs within the shaded region. From the discussion above, we conclude that the pairing amplitude is nonzero when the oscillations onset. Above H_{m2}, the oscillations exist in the vortex liquid state where the magnetization is manifestly diamagnetic. The coexistence of the dHvA oscillations with diamagnetic response was previously observed in ref. 15.

Magnetic Phase Diagram and Discussion

The combined experiments uncover a rather rich magnetic phase diagram that allows us to relate the charge-ordering field scales obtained by NMR and X-ray diffraction to the vortex states in underdoped YBCO. In Fig. 8 the melting field H_m, which defines the stability region of the vortex solid, increases monotonically as

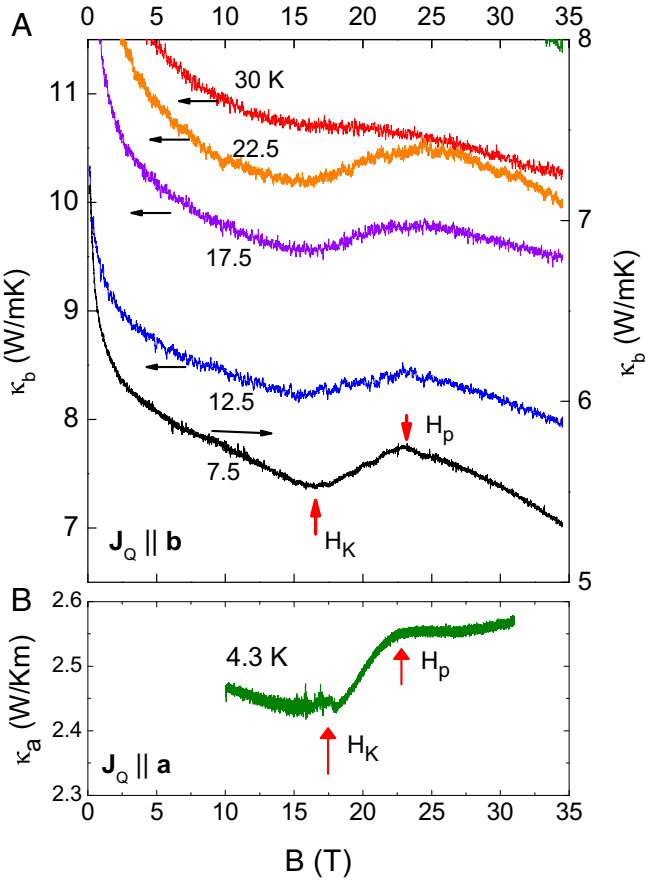

Fig. 6. Expanded views of curves of the thermal conductivity at selected T. (*A*) Traces of κ_b measured in sample 4 measured in a field **H**||**c** with the heat current density $\mathbf{J}_Q$||**b** (chain axis). The vertical scale for 7.5 K is on the right axes. At the fields H_K and H_p (arrows), κ_b exhibits a distinct changes of slope. (*B*) κ_a measured at 4.3 K in sample 5 with **H**||**c** and $\mathbf{J}_Q$||**a**.

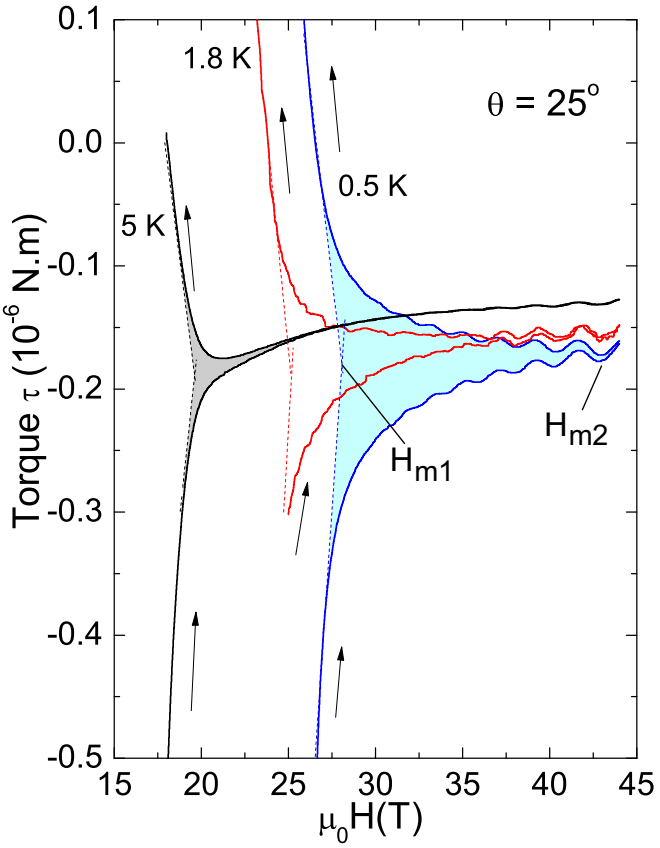

Fig. 7. Hystereses in the curves of the torque τ vs. H in high fields at low T in sample 3. At each T, hysteretic behavior between the sweep-up and -down curves defines the field region in which the vortex solid is stable (arrows indicate field sweep directions). For the curves at 15 K (black curves), the rapid closing of the hysteresis loop with increasing H (gap between the upper and lower branches) signals the melting of the vortex solid. The nexus of the linear extrapolations of the two branches (dashed lines) defines the melting field $H_{m1} \sim 19.5$ T. However, a small wedge representing vortex solid 2 exists to $H_{m2} \sim 25$ T (shaded gray). At 0.5 K, the vortex solid 2 region has expanded considerably (shaded light blue). At the three temperatures, dHvA oscillations are resolved. At 0.5 K, they onset in the vortex solid 2 region. We note that at all fields up to 45 T, the magnetization is manifestly strongly diamagnetic ($\tau < 0$). Hence, at each T, the region above H_{m2} is a stable vortex liquid with finite pair amplitude.

T decreases below T_c (black circles). At ~9 K, it bifurcates into the two curves H_{m1} and H_{m2}. Whereas H_{m1} intercepts the H axis at ~25 T at 0.5 K (our lowest T), the higher field H_{m2} rises steeply to exceed 40 T at 0.5 K. The two vortex solid phases separated by H_{m1} are shaded differently and labeled as 1 and 2. As discussed above, H_{m1} —estimated by a linear extrapolation of the sweep-up and sweep-down curves of M_d vs. H—measures the field at which the vortex solid loses most of its shear rigidity. Above H_{m1}, however, substantial irreversibility remains which implies that the vortex solid remains. This is most apparent in the M_d –H curves at 0.5 K (Fig. 7).

One of our key conclusions is that the vortex liquid is stable in the region shaded light blue in Fig. 8. This region extends from H_m to our maximum $H_z \sim 41$ T and up to temperatures above T_c. We emphasize that even when hysteretic behavior vanishes in the M_d –H curves, the magnetization remains negative and strongly T-dependent (see especially the curve at 0.5 K in Fig. 7). The reversible, T-dependent diamagnetism is the experimental hallmark of the vortex liquid. The pair amplitude is nonzero in the vortex liquid although dissipation is large because the vortex liquid—lacking a finite shear modulus—cannot be pinned by disorder. The picture of a relatively small $H_m(T)$, together with the very large pairing energy scale that allows the vortex liquid to survive to very large H, is closely similar to that in other underdoped cuprates (12, 13, 17–20).

In Fig. 8, we have also plotted the field $H_K(T)$ inferred from χ_d (blue squares) with the dashed line drawn as a guide. The red triangles represent H_K inferred from κ_{xx}. As T decreases from 35 to 4 K, H_K is nearly T-independent. Below 6 K, H_K intersects the melting curve. We identify H_K with the onset of LRO in the CDW as detected by X-ray diffraction (15 T at 10 K) (9). Three-dimensional ordering of the CDW onsets near 15 T although strong 2D fluctuations appear at 10 T (10). In Wu et al. (8), the splitting of the NMR ^{17}O lines onsets at a lower field (10 T for $P = 0.109$), but saturates at a field close to our H_p (23 T). Below 40 K, the field scale B_{co} extracted from an ultrasonic experiment (6) lies slightly higher than our H_K curve (although the difference may arise from the combined uncertainties). The present results imply that the initial onset of static charge ordering has no observable effect on the melting field of the vortex solid.

The higher field H_p inferred from κ_{xx} (also nearly T-independent) is plotted as open triangles. In the limit $T \to 0$, it extrapolates to a value 24 ± 1 T close to the intercept of H_{m1}. H_p is close to the value at which the splitting of the NMR lines saturates.

A recent experiment in underdoped YBCO (with $p = 0.11$) has observed that κ_{xx} at 1.8 K rises to a distinct peak at ~ 23 T (7). The authors interpret the peak as the true upper critical field H_{c2}. However, the present results show that at $T = 0.5$ K, the vortex solid exists up to 41 T while the vortex liquid persists to even higher H. Hence the pair condensate with strong superconducting

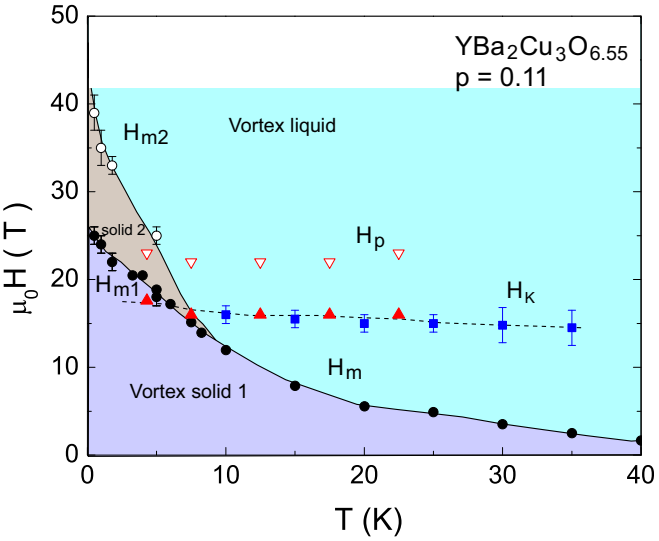

Fig. 8. Magnetic phase diagram in untwinned $YBa_2Cu_3O_y$ ($y = 6.55$) inferred from magnetization and the thermal conductivity. Given the 2D nature of the transition curves, the vertical axis refers to the z component of **H** applied in the torque experiments (for κ_{xx} measurements, **H** is always $\|\hat{z}$). Above ~ 8 K, the vortex solid is stable below the melting field H_m (solid circles). Below ~ 8 K, the H_m curve splits into two branches: H_{m1} (solid circles) and H_{m2} (open circles). The vortex solid 1 below H_{m1} displays a large critical current density J_c and shear modulus, whereas the solid 2 ($H_{m1} < H < H_{m2}$) has a much smaller J_c but survives to ~ 41 T at 0.5 K. Throughout, the vortex-liquid state is stable to at least 41 T (region shaded light blue), but likely much higher judging from the trend in M_d vs. H. The nearly T-independent kink field H_K, identified as the onset of static charge order, is plotted as blue squares (inferred from χ_d) and as red solid triangles (from κ_a and κ_b). It intersects H_{m1} without affecting the melting (to our resolution). The field scale H_p (open triangles, derived from κ_a and κ_b) appears to terminate at the lower melting field H_{m1} in the limit $T \to 0$. At 0.5 K, the dHvA oscillations onset near 25 T (coexist with the vortex liquid below ~ 41 T).

PHYSICS

correlations survives well above 23 T. A similar inference based on the X-ray peak intensity at 28 T was reported by Gerber et al. (9).

The different experimental probes provide a picture that is richer and more interesting than the identification (7) of a mean-field Bardeen–Cooper–Schrieffer-type transition at which the pair condensate simply vanishes (at 23 T). In a d-wave superconductor, the electronic thermal conductivity κ^e (we suppress the subscript xx) is overwhelmingly dominated by the quasiparticle (qp) population at the nodes (at $T \ll T_c$). Hence changes to κ^e predominantly reflect changes to the fermi surface (FS) at or close to the node (example, closing of the gap along an FS arc or creation of a small pocket). Moreover, the curves in Fig. 6 show that raising T above 25 K suppresses all traces of the step change in κ_{xx} (5% at 4.3 K). Thermal broadening of the broad peak at H_K in χ_d is equally rapid (Fig. 3). This provides direct evidence that the FS changes at the node involve energy scales of ~1–2 meV, far smaller than the gap amplitude Δ_0 at the antinodes. In Fig. 8, the convergence of the lower melting curve H_{m1} (which separates the two vortex solids) and the cross-over curve H_p to values close to 23 T as $T \to 0$ suggests to us that, as the 3D CDW amplitude grows, the pair condensate undergoes an abrupt transition at 23–24 T to accommodate the competing CDW (this strongly affects the vortex solid shear modulus as discussed below). We propose that the peak in κ^e reflects changes (at energy scales of 1–2 meV) to the nodal states caused by the CDW transition, rather than suppression of the gap amplitude Δ_0 (40–80 meV).

In ref. 7, a mean-field H_{c2} curve extending from 23 T at 2 K to zero at T_c is drawn without reference to experiment. The magnetization curves in Fig. 1 are incompatible with such a mean-field curve (M_d varies smoothly through the proposed H_{c2} curve; see arrow labeled "MF"). (We extended measurements of both κ_{xx} and the thermal Hall conductivity κ_{xy} to lower T. For the doping level in our crystal, we observe at 0.5 K a sharp cusp in κ_{xy} at 18 T, followed by the onset of a large negative thermal Hall contribution. The critical field 18 T is lower than 23 T, but consistent... with the dashed line linking solid triangles in Fig. 8. As 18 T lies below H_{m1}, the system is well within the vortex solid 1 phase when the transition affecting the nodal qp states occurs.)

An interesting issue raised by the phase diagram is the fate of both the vortex solid and liquid in the quantum limit $T \to 0$ (21). As remarked above (Fig. 7), the rapid expansion of the vortex solid 2 phase (between H_{m1} and H_{m2}) suggests that the pair condensate may modify its pairing pattern to accommodate the static CDW. Several groups have proposed (22–27) either the pair-density–wave formation or the related Fulde–Ferrell–Larkin–Ovchinikov state (28). It is intriguing that when $T \to 0$, the transition at $H_{m1} \sim 24$ T also occurs close to the field H_p. The present experiments show that this allows the vortex solid to survive to much higher H at the cost of a substantial decrease in its shear modulus.

The question whether the vortex liquid exists as a stable quantum phase at $T = 0$ is resolvable by extending the torque measurements below 0.1 K to fields above 41 T. The properties of the quantum vortex liquid (in an ultraclean superconductor) are largely unknown but may become accessible to torque magnetometry at mK temperatures in the near future. The existence of the vortex liquid to fields substantially higher than 41 T implies that the Cooper pair amplitude in underdoped YBCO is too strong to be suppressed at these field scales.

ACKNOWLEDGMENTS. The research of L.L. is supported by the US Department of Energy, Office of Basic Energy Sciences, Division of Materials Sciences and Engineering under Award DE-SC0008110 (high-field magnetization). M.H. and N.P.O. were supported by National Science Foundation (NSF)-MRSEC (Materials Research Science and Engineering Centers) Grant DMR 1420541 and the Gordon and Betty Moore Foundations EPiQS (Emergent Phenomena in Quantum Systems) Initiative through Grant GBMF4539 (thermal conductivity and analysis). The experiments were performed at the National High Magnetic Field Laboratory, which is supported by NSF Cooperative Agreement DMR-1157490, the State of Florida, and the US Department of Energy.

1. Wu T, et al. (2011) Magnetic-field-induced charge-stripe order in the high-temperature superconductor YBa2Cu3Oy.$_{23}$ *Nature* 477(7363):191–194.
2. Ghiringhelli G, et al. (2012) Long-range incommensurate charge fluctuations in (Y,Nd)Ba2Cu3O(6+x). *Science* 337(6096):821–825.
3. Chang J, et al. (2012) Direct observation of competition between superconductivity and charge density wave order in YBa2Cu3O6.67. *Nat Phys* 8:871–876.
4. Blanco-Canosa S, et al. (2013) Momentum-dependent charge correlations in YBa2Cu3O6+δ superconductors probed by resonant X-ray scattering: Evidence for three competing phases. *Phys Rev Lett* 110(18):187001.
5. Blackburn E, et al. (2013) X-ray diffraction observations of a charge-density-wave order in superconducting ortho-II YBa2Cu3O6.54 single crystals in zero magnetic field. *Phys Rev Lett* 110(13):137004.
6. LeBoeuf D, et al. (2013) Thermodynamic phase diagram of static charge order in underdoped YBa2Cu3Oy. *Nat Phys* 9:79–83.
7. Grissonnanche G, et al. (2014) Direct measurement of the upper critical field in cuprate superconductors. *Nat Commun* 5:3280.
8. Wu T, et al. (2013) Emergence of charge order from the vortex state of a high-temperature superconductor. *Nat Commun* 4:2113.
9. Gerber S, et al. (2015) Three-dimensional charge density wave order in YBa2Cu3O6.67 at high magnetic fields. *Science* 350(6263):949–952.
10. Chang J, et al. (2016) Magnetic field controlled charge density wave coupling in underdoped YBa2Cu3O6+x. *Nat Commun* 7:11494.
11. Le Tacon M, et al. (2014) Inelastic X-ray scattering in $YBa_2Cu_3O_{6.6}$ reveals giant phonon anomalies and elastic central peak due to charge-density-wave formation. *Nat Phys* 10:52.
12. Wang Y, et al. (2005) Field-enhanced diamagnetism in the pseudogap state of the cuprate Bi2Sr2CaCu2O(8+delta) superconductor in an intense magnetic field. *Phys Rev Lett* 95(24):247002.
13. Li L, et al. (2010) Diamagnetism and Cooper pairing above Tc in cuprates. *Phys Rev B* 81:054510.
14. Shoenberg D (1984) *Magnetic Oscillations in Metals* (Cambridge Univ Press, Cambridge, UK).
15. Sebastian SE, et al. (2008) A multi-component Fermi surface in the vortex state of an underdoped high-Tc superconductor. *Nature* 454(7201):200–203.
16. Doiron-Leyraud N, et al. (2007) Quantum oscillations and the Fermi surface in an underdoped high-Tc superconductor. *Nature* 447(7144):565–568.
17. Wang Y, Li L, Ong NP (2006) Nernst effect in high-Tc superconductors. *Phys Rev B* 73: 024510.
18. Kivelson S, Fradkin E (2010) Viewpoint: Fluctuation diamagnetism in high-temperature superconductors. *Physics (College Park Md)* 3:15.
19. Dubroka A, et al. (2011) Evidence of a precursor superconducting phase at temperatures as high as 180 K in RBa2Cu3O(7-δ) (R=Y, Gd, Eu) superconducting crystals from infrared spectroscopy. *Phys Rev Lett* 106(4):047006.
20. Jaudet C, et al. (2008) de Haas-van Alphen oscillations in the underdoped high-temperature superconductor YBa2Cu3O6.5. *Phys Rev Lett* 100(18):187005.
21. Li L, Checkelsky J, Komiya S, Ando Y, Ong N (2007) Low temperature vortex liquid in $La_{2-x}Sr_xCuO$. *Nat Phys* 3:311–314.
22. Tranquada JM, et al. (2008) Evidence for unusual superconducting correlations coexisting with stripe order in $La_{1.875}Ba_{0.125}CuO_4$. *Phys Rev B* 78:174529.
23. Himeda A, Kato T, Ogata M (2002) Stripe states with spatially oscillating d-wave superconductivity in the two-dimensional t-t′-J model. *Phys Rev Lett* 88(11):117001.
24. Chen HD, Vafek O, Yazdani A, Zhang SC (2004) Pair density wave in the pseudogap state of high temperature superconductors. *Phys Rev Lett* 93(18):187002.
25. Lee PA (2014) Amperean pairing and the pseudogap phase of cuprate superconductors. *Phys Rev X* 4:031017.
26. Fradkin E, Kivelson SK, Tranquada JM (2015) Colloquium: Theory of intertwined orders in high temperature superconductors. *Rev Mod Phys* 87:457.
27. Hamidian MH, et al. (2016) Detection of a Cooper-pair density wave in Bi2Sr2CaCu2O8+x. *Nature* 532(7599):343–347.
28. Fulde P, Ferrell RA (1964) Superconductivity in a strong spin-exchange field. *Phys Rev* 135:A550.